SAND2013-3293C
Proceedings of the ASME 2013 International Design Engineering Technical Conferences & Computers and Information in Engineering Conference
IDETC/CIE 2013
August 4-7, 2013, Portland, Oregon, USA

13257

APPLICATION OF VISCOUS AND IWAN MODAL DAMPING MODELS TO EXPERIMENTAL MEASUREMENTS FROM BOLTED STRUCTURES

Brandon J. Deaner
Graduate Research Assistant
Department of Engineering Physics
University of Wisconsin-Madison
534 Engineering Research Building
1500 Engineering Drive
Madison, Wisconsin 53706
bdeaner@wisc.edu

Matthew S. Allen
Assistant Professor
Department of Engineering Physics
University of Wisconsin-Madison
535 Engineering Research Building
1500 Engineering Drive
Madison, Wisconsin 53706
msallen@engr.wisc.edu

Michael J. Starr
Component Science and Mechanics
Sandia National Laboratories
P.O. Box 5800
Albuquerque, NM, 87185
mjstarr@sandia.gov

Daniel J. Segalman
Multi-Physics Modeling & Simulation Department
Sandia National Laboratories
P.O. Box 969, Mail Stop 9042
Livermore, CA, 94551
djsegal@sandia.gov

ABSTRACT

Measurements are presented from a two-beam structure with several bolted interfaces to characterize the nonlinear damping introduced by the joints. The measurements (at force levels below macro-slip) reveal that each underlying mode of the structure is well approximated by a single degree-of-freedom system with a nonlinear mechanical joint. At low enough force levels the measurements show dissipation that scales as the second power of the applied force, agreeing with theory for a linear viscously damped system. This is attributed to linear viscous behavior of the material and/or damping provided by the support structure, which simulates free-free boundary conditions. At larger force levels the damping is observed to behave nonlinearly, suggesting that damping from the mechanical joints is dominant. A model is presented that captures these effects, consisting of a spring and viscous damping element in parallel with a 4-Parameter Iwan model. The parameters of this model are identified for each mode of the structure and comparisons suggest that the model captures the linear and nonlinear damping accurately over a range of forcing levels.

INTRODUCTION

Mechanical joints are known to be a major source of damping in jointed structures. However, the amplitude dependence of damping in mechanical joints has proven to be quite difficult to predict. For many systems, linear damping models seem to capture the response of a structure near the calibrated force level. However, that approach can be over-conservative or even erroneous since a linear model does not capture the amplitude dependence of the damping. It would be far better to understand how mechanical joints behave over a range of forces so that the response of a jointed structure can be modeled accurately.

From ring-down data of free-free structures, some trends have emerged that provide insight into modeling the damping of mechanical joints. For instance, when testing a bolted structure at very low force levels, the damping of mechanical joints can be so light that it is difficult to detect experimentally. Thus, the overall measured damping is likely to be linear and is due to material damping and from the suspension support conditions of the experimental set-up. Yet, at larger force levels, the damping is often observed to be nonlinear, meaning the damping from the mechanical joints is significant. Consequently, this work seeks to develop a model that captures

the linear damping at low force levels and nonlinear damping at large force levels.

Mechanical joints are said to be undergoing micro-slip when the joint as a whole remains intact but small slip displacements occur at the outskirts of the contact patch causing frictional energy loss in the system [1]. When this is the case the overall response of the structure is often well approximated with a linear modal model and such a model is used in this work to capture the response.

To capture the nonlinear damping, a 4-Parameter Iwan model [2] will be used. This constitutive model accounts for the key characteristics of the joint's response including the power law energy dissipation seen in the micro-slip region. In the past decade, the 4-Parameter Iwan model has been implemented to predict the vibration of structures with a few discrete joints [3, 4]. However, when modeling individual joints, each joint requires a unique set of parameters, which means that one must deduce hundreds or even thousands of joint parameters to describe a system of interest. On the other hand, when a small number of modes are active in a response, recent measurements have suggested that a simpler model may be adequate. Segalman et al. recently applied the 4-Parameter Iwan model in a modal framework to describe both discrete joint simulations and experimental data from structures with bolted joints [5, 6].

This work extends the modal Iwan framework adding some features that are necessary to approximate real experimental data. The 4-Parameter Iwan model only accounts for the energy dissipation associated with the mechanical joints of the system, which dominate at large force levels. However, at low force levels, the damping of the system is dominated by material damping of the structure and damping from the suspension support conditions of the experimental set-up. These linear sources of damping must be accounted for, when fitting experimental data. In this work, the linear modal damping will be accounted for using a viscous damper in parallel with the 4-Parameter Iwan modal model. Experimental measurements are presented and are found to be well represented by this model.

NOMENCLATURE

q_0	Modal amplitude of displacement
F_{VD}	Force in the viscous damper
C	Modal viscous damping coefficient
F_{LE}	Force in the linear elastic spring
K_∞	Linear elastic stiffness of the system
F_{Iwan}	Force in the Iwan joint
R, χ	Coefficient and exponent in the Iwan distribution function
F_S	Force necessary to cause macro-slip of joint
K_T	Stiffness of the Iwan joint
β	Iwan parameter related to level of energy dissipation and shape of energy dissipation curve
D_{Model}	Energy dissipated by the model
K_{Model}	Stiffness of the model
V(t)	Analytic signal
KE	Kinetic Energy
D_{Exp}	Energy dissipated by experimental data
K_{Exp}	Stiffness of the experimental data
f	Total optimization objective function
f_D	Energy dissipation objective function
f_K	Stiffness objective function

MODAL MODEL

Segalman proposed that nonlinear energy dissipation due to bolted joints could be applied on a mode-by-mode basis, using the 4-parameter Iwan constitutive model [5]. In general, the nonlinearity that joints introduce can couple the modes of a system so that modes in the traditional linear sense can not be defined. However, damping is often relatively weak effect and experiments have often shown that the modes of structures with joints are typically quite linear, suggesting that one might be able to model the structure as a collection of uncoupled linear modes, each with nonlinear damping characteristics [6].

Under these assumptions, each modal degree-of-freedom is modeled by a single degree-of-freedom oscillator, as shown in Fig. 1, with a 4-parameter Iwan model in parallel with a viscous damper and an elastic spring. Note that the displacement of the mass is not a physical displacement but the modal displacement or modal amplitude, q, of the mode of interest. The mode vectors are assumed mass normalized so the mass is taken to be unity.

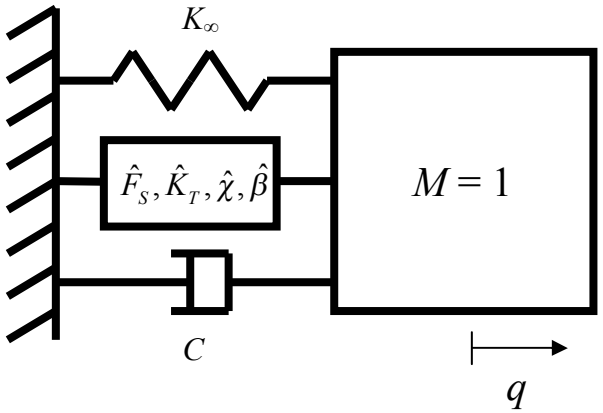

Fig. 1 Schematic of the model for each modal degree of freedom. Each mode has a unique set of Iwan parameters that characterize its nonlinear damping and a viscous damper that characterizes the linear damping.

The 4-parameter Iwan model has parameters $\{F_S, K_T, \chi, \beta\}$ where F_S is the joint force necessary to initiate macro-slip, K_T is the stiffness of the joint, χ is directly related to the slope of the energy dissipation in the micro-slip regime, and β relates to the level of energy dissipation and the shape of the energy dissipation curve as the macro-slip force is approached. Finally, the viscous damper has a coefficient, C, and the linear elastic spring stiffness is K_∞. Note that all of the parameters are defined in modal and not physical space.

ENERGY DISSIPATION AND STIFFNESS

Model

The energy dissipation for the modal model seen in Fig. 1 can be solved for and used to fit experimental data. Assuming a harmonic load is applied to the mass and the system is at steady-state, the mass will oscillate as

$$q = q_0 \sin(\omega t) \tag{1}$$

where q_0 is the modal displacement amplitude and ω is the response frequency. The force in the viscous damper can be written as

$$F_{VD} = C\dot{q} \tag{2}$$

where C is the viscous damping coefficient. The force in the linear elastic spring takes the form

$$F_{LE} = K_\infty q \tag{3}$$

where K_∞ is the spring stiffness. The force in the Iwan joint is given in [2]. Assuming that the amplitude of motion is small, $q_0 < \phi_{\max}$ or in other words the Iwan joint is undergoing micro-slip, the force in the Iwan model can be approximated as

$$F_{Iwan} = \frac{Rq^{\chi+2}}{\chi+2} \tag{4}$$

where R is a coefficient that describes the population distribution of the parallel-series Iwan system [2]. These forces can be added, $F_{Total} = F_{VD} + F_{LE} + F_{Iwan}$, multiplied by the modal velocity and integrated over one period as follows,

$$D_{Model} = \int_0^{\frac{2\pi}{\omega}} F_{Total}\dot{q}\, dt \tag{5}$$

to obtain the energy dissipation per cycle, D_{Model}.

$$D_{Model} \approx \frac{4Rq_0^{\chi+3}}{(\chi+3)(\chi+2)} + \pi\omega C q_0^2 \tag{6}$$

Notice that the energy dissipation depends on the maximum modal amplitude q_0 and that the linear elastic spring does not contribute to the energy dissipated as one would expect.

From [2], the secant stiffness of the Iwan joint at large amplitudes of oscillation can be approximated as:

$$K_{Model} \approx K_T\left(1 - \frac{r^{\chi+1}}{(\chi+2)(\beta+1)}\right) + K_\infty \tag{7}$$

where

$$r = \frac{q_0 K_T\left(\beta + \frac{\chi+1}{\chi+2}\right)}{F_S(1+\beta)} \tag{8}$$

Note that both D_{Model} and K_{Model} as presented above are approximations to the actual dissipation and stiffness, and are valid in the micro-slip regime only. In order to obtain the actual dissipation and stiffness, the Iwan model can be integrated in time and then the actual dissipation and stiffness can be deduced. However, as discussed in later sections, D_{Model} and K_{Model} are used to decrease computational time when solving an optimization problem to find the modal Iwan parameters that best fit the data.

Processing Experimental Measurements

The energy dissipation for each mode of a system can be computed from measurements of its free response. The procedure for processing measurements was presented in [6] and will be reviewed briefly below.

First, a filter is used to isolate an individual modal response. The authors have used both modal filters [7] and standard, infinite impulse response band-pass filters [8] for this purpose and other possibilities certainly exist. The Hilbert Transform [9] is then used to compute the instantaneous damping and frequency of the system. This process requires some care since the basic Hilbert transform performs very poorly in the presence of noise. This work uses a variant where curve fitting is used [10] to smooth the instantaneous amplitude and phase found by a standard Hilbert transform and then the curve fit model can be differentiated to estimate the instantaneous frequency, as explained below.

One obtains an analytic representation of the modal response, denoted $V(t)$, by adding the Hilbert transform of the modal velocity, $\tilde{v}(t)$, to the measured modal velocity of the mode of interest, $v(t) = \dot{q}_r(t)$ as follows

$$V(t) = v(t) + i\tilde{v}(t) \tag{9}$$

The magnitude of the analytic signal is the decay envelope of the response and is approximated by

$$|V(t)| = V_0\, e^{P(t)} \tag{10}$$

where V_0 is the initial amplitude. To maintain similarity with a linear system, the product of the natural frequency, $\omega_n(t)$, and the coefficient of critical damping, $\zeta(t)$, is defined to be the time derivative of $P(t)$.

$$\frac{dP(t)}{dt} = \alpha(t) \approx -\zeta(t)\omega_n(t) \tag{11}$$

The instantaneous phase is the complex angle of the analytic signal, which can be obtained using the following (provided that a four-quadrant arctangent formula is used).

$$\varphi(t) = \tan^{-1}\left(\frac{\tilde{v}(t)}{v(t)}\right) \tag{12}$$

The measured phase and the natural logarithm of the decay envelope are then smoothed by fitting a polynomial to the data.

In addition, before the data is fit, the beginning and end of the data are deleted since they tend to be contaminated by end effects in the Hilbert Transform. The time-derivative of the phase then gives the instantaneous damped natural frequency.

$$\omega_d(t) = \frac{d\varphi(t)}{dt} \tag{13}$$

The time varying natural frequency is then found using the following equation:

$$\omega_n(t) = \sqrt{\left(\omega_d(t)\right)^2 + \left(-\alpha(t)\right)^2} \tag{14}$$

Now the energy dissipation per cycle can be calculated from the change in kinetic energy over one cycle. The amplitude of the kinetic energy can be written as,

$$KE = \frac{1}{2} M \left|V(t)\right|^2 \tag{15}$$

and the change in the kinetic energy is found by taking the derivative of this expression. Since the kinetic energy and its derivative are quite smooth, the energy dissipated per cycle, D_{Exp}, can be approximated by simply multiplying dKE/dt by the period ($2\pi/\omega_n(t)$) (e.g. using a trapezoid rule to integrate the power dissipated as a function of time).

$$D_{Exp} \approx \frac{2\pi}{\omega_d}\frac{dKE}{dt} = \frac{2\pi}{\omega_d}\frac{dP(t)}{dt}\left|V(t)\right|^2 \tag{16}$$

Finally, the experimental modal stiffness is solved for by squaring the time varying natural frequency.

$$K_{Exp} = \omega_n(t)^2 \tag{17}$$

EXPERIMENTS ON TWO-BEAM STRUCTURE

The proposed damping model was assessed using experimental measurements on a structure comprise of two beams bolted together. The structure is tested in free-free conditions, and care was taken to design the experimental setup to minimize the effect of damping associated with the boundary conditions. Free boundary conditions were used because any other choice, e.g. clamped, would add even more damping to the system.

Test Structure

In this work, the structure consisted of two beams bolted together with four bolts as shown in Fig. 2. The two beams, each with dimensions 0.508m × 0.051m × 0.006m (20" × 2" × 0.25") were fastened together with 1/4"-28 fine-threaded bolts and all components were made of AISI 304 stainless steel. The bolts were tightened to three different torque levels in these tests: 1.13, 3.39, 5.65 N-m (10, 30, and 50 in-lbs). For reference, the Society of Automotive Engineers (SAE) provides the general torque specification for this type of bolt to be approximately 8.5 N-m (75.0 in-lbs) [11] which results in bolt preload force of approximately 6700 N (1500 lbf). The largest torque used here was somewhat lower than this specification, but, as will be shown, this structure became quite linear for the range of excitation forces that were practical with this setup, so the bolts were kept somewhat loose to accentuate the nonlinearity. Future works will explore methods of exciting the structure with higher force levels (closer to what might be seen in the applications of interest) so that more realistic torques can be used.

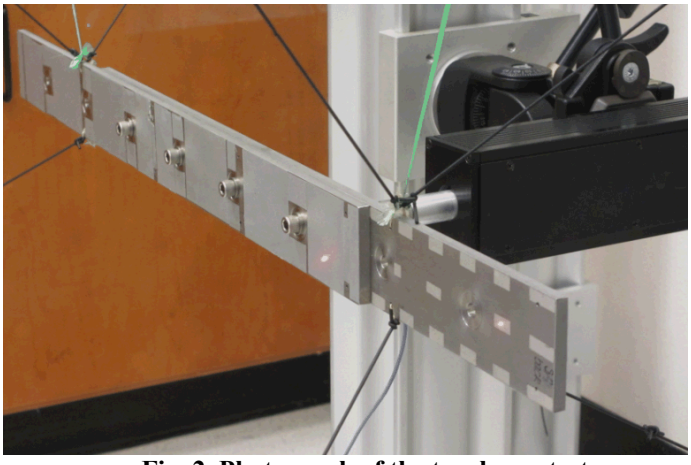

Fig. 2 Photograph of the two beam test structure.

Experimental Setup

The dynamic response of the two beam structure was measured using a Polytec scanning laser Doppler vibrometer (PSV-400) to measure the response at 70 points on the structure. A Polytec single point laser Doppler vibrometer (OFV-534) was used to measure at a reference point to verify that the hammer hits were consistent. The reference laser was positioned close to the impact force location as seen in Fig. 2.

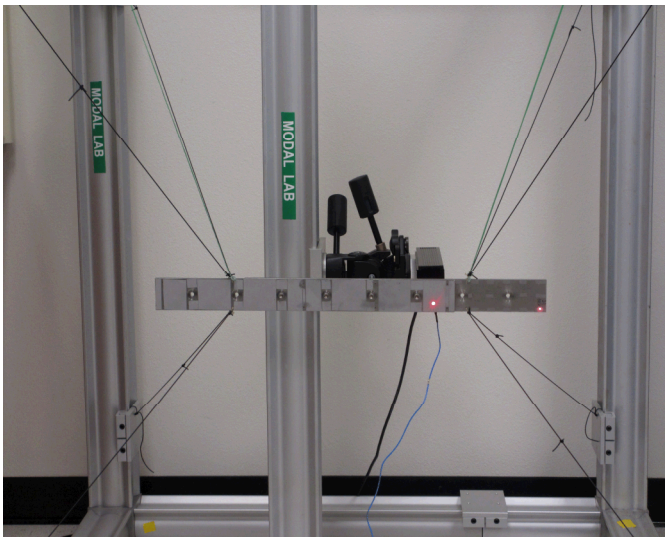

Fig. 3 Photograph of the suspension setup for the two beam test structure.

The structure is suspended by 2 strings that support the weight of the structure and the 8 bungee cords prevent excessive rigid-body motion. The bungees and strings were connected to the beam at locations where the odd bending modes have little motion in order to minimize damping in those modes.

An Alta Solutions automated impact hammer with a nylon hammer tip was used to supply the impact force, which is measured by a force gauge attached between the hammer and the hammer tip. Additional measurements were taken at higher force levels using a modal hammer; however, the supplied impact force was not as consistent. The mean and standard deviation of the maximum impact force for all of the torque levels and force levels that were used in this study are shown in Table 1.

Table 1: Mean and standard deviation of the maximum impact force for all 70 measurements.

Torque (N-m)	Hammer Level	Mean Impact Force (N)	Standard Deviation of Impact Force (N)
1.13	1 (lowest)	20.24	0.80
1.13	2	32.77	0.27
1.13	3	86.44	0.68
1.13	4 (highest)	288.57	6.10
3.39	1 (lowest)	24.1	0.38
3.39	2	30.9	0.51
3.39	3	52.8	3.84
3.39	4 (highest)	180.1	58.24
3.39	Modal Hammer	1444.5	139.34
5.65	1 (lowest)	20.8	0.44
5.65	2	36.5	0.28
5.65	3	60.3	0.61
5.65	4 (highest)	238.6	15.30
5.65	Modal Hammer	1392.1	172.48

The automatic hammer provides a range of force levels between approximately 20 and 300 N. However, the force level is dependent upon the distance between the hammer tip and the beam and the voltage supplied to the automatic hammer. For these reasons, the lowest and highest force varies for each measurement. For the automatic hammer, the standard deviation tends to increase as the force level is increased. At the highest force level, the automatic hammer has a large spread for all the torque levels especially the 3.39 N-m torque. The modal hammer is able to reach much higher force levels (approximately 1400 N); however, the standard deviations are much larger when compared to the automatic hammer.

Lab Setup Challenges

The damping ratios of a freely supported structure are sensitive to the support conditions, as was explored in detail by Carne, Griffith, and Casias in [12]. Therefore, special attention must be given to the support conditions to assure that the damping that they add does not contaminate the results. Initially, the two beam structures were suspended by two strings that act as pendulum supports as was done in [12]. These support conditions contributed very little damping to the system; however, several obstacles lead to the addition of 8 soft bungee cords in addition to the two strings.

Specifically, the velocity of the beam was measured with a scanning laser Doppler vibrometer in order to eliminate any damping associated with the cables that must be added if accelerometers were used. Hence, if the beam swings significantly in its pendulum mode, the point which the laser is measuring may change significantly during the measurement. Also, an automated hammer was used to excite the beam, but the hammer only retracts about 2.5 centimeters (1 inch) after impact. As a result, the pendulum motion of the beam caused almost unavoidable double hits when the bungee cords were not present. Finally, in the processing described subsequently, it is important for the automatic hammer to apply a highly consistent impact force. Any ambient swinging of the beam caused the impact forces to vary from test to test. When the bungee cords were not present, it was extremely difficult and time consuming to try to manually eliminate the ambient swinging. For these reasons, soft bungee cords were added to the setup to suppress the rigid body motion of the beam while attempting to add as little stiffness and damping as possible to the system. The final set up was similar to that used in [13] and is shown in **Error! Reference source not found.**Fig. 3. This setup was used for all of the measurements shown in this paper.

A comparison was done to ensure that the addition of bungee cords did not add significant damping to the system. A monolithic structure, without interfaces and bolts, was chosen to ensure that the measured damping was only due to the structure itself and the support conditions. A single beam was suspended with two strings with and without the bungees cords and the damping ratios for the first three modes were found using the Algorithm of Mode Isolation (AMI) [14, 15] and are presented in Table 2.

Table 2: Modal Damping Ratios for a single beam with and without bungees.

Elastic Mode #	ζ without bungees (%)	ζ with bungees (%)
1	0.010	0.016
2	0.025	0.057
3	0.020	0.044

The damping of all of the modes is very light, as one would expect for a monolithic structure. When the bungees were added to the setup, the damping ratios for all modes increased by about a factor of two. The bungees and strings were connected to the beam at locations where the motion of the symmetric or odd bending modes is minimum, to minimize

the damping that is added to those modes, but these locations are expected to add some damping to the second mode. However, the results show that the supports added some damping to the first and third modes as well. These damping ratios are an average of the damping ratios found at a range of force levels; the structure is linear so the force level did not have a significant impact on the damping

Table 3: Averaged Modal Damping Ratios for the two beam test structure.

Elastic Mode #	1.13 N-m Torque, ζ (%)	3.39 N-m Torque, ζ (%)	5.65 N-m Torque, ζ (%)
1	1.2	0.29	0.16
2	0.57	0.48	0.26
3	0.31	0.16	0.11

For comparison, the approximate linear modal damping ratios for the two beam structure at each of the three torque levels are presented in Table 3. Due to the nonlinearity introduced by the joints in the two beam structure, the damping ratios would seem to change with the amount of excitation applied. The damping ratios presented in Table 3 are averaged over the range of force excitations used in these experiments, and hence they represent a linear fit to a structure which is known to be nonlinear and this probably does introduce some distortion. For each mode, the damping is observed to decrease as the bolt torque increases. This was expected since increasing the bolt torque inhibits micro-slip and hence should decrease the measured damping. However, even at the tightest bolt torque (5.65 N-m) the modal damping ratios have increased by a factors of 10, 4.5, and 2.5 for the first three modes respectively. Therefore, it seems that a significant portion of the measured damping is due to the joints in the structure in addition to the material damping and the damping provided by the support conditions.

Lab Data Processing

A couple of approaches were explored to extract modal velocity ring-downs from the laboratory data. Mass normalized mode shapes were found by fitting a linear modal model with the Algorithm of Mode Isolation (AMI) [14, 15]. Then the mode shapes were used in a modal filter.

$$\dot{x} = \Phi \dot{q} \tag{18}$$

However, when using a modal filter the modal responses showed clear evidence of frequency content due to other modes, which would contaminate the Hilbert transform analysis. Since this system's modes are well separated, the modes were isolated by creating a band pass filter to isolate each mode, as was done in [16], using a fourth order Butterworth filter. The filtered responses were then divided by the corresponding mass normalized mode shape at each point, j, to estimate the modal displacement as follows, $\dot{q}_r = \dot{x}_j / \Phi_{jr}$ There were 70 measurement points which were then averaged to estimate a single modal velocity for each mode. Some measurement points were excluded from averaging process if the mode was excited to heavily or not sufficiently. A trimmed mean was used to determine which measurements to keep. The trimmed mean procedure excluded 8 high and low outliers from the set of 70 measurements points. All measurement points whose maximum velocity was within 50 percent of the trimmed mean were kept. Resulting statistics on the filtered impact hammer data is presented in Table 4.

Table 4: Mean and standard deviation of the maximum impact force for all filtered measurements.

Torque (N-m)	Hammer Level	Mean Impact Force (N)	Standard Deviation of Impact Force (N)
1.13	1 (lowest)	20.0	0.088
1.13	2	32.8	0.025
1.13	3	86.5	0.041
1.13	4 (highest)	289.3	0.213
3.39	1 (lowest)	24.2	0.013
3.39	2	30.8	0.019
3.39	3	52.7	0.125
3.39	4 (highest)	191.3	1.585
3.39	Modal Hammer	1475.7	3.081
5.65	1 (lowest)	20.9	0.009
5.65	2	36.5	0.005
5.65	3	60.3	0.011
5.65	4 (highest)	237.2	0.310
5.65	Modal Hammer	1400.4	3.225

All of the filtered standard deviations in Table 4 are smaller than the initial standard deviations shown in Table 1. Again, for the automatic hammer, the standard deviation tends to increase as the force level is increased. Yet, at the highest force level, the automatic hammer has a much more reasonable maximum standard deviation of 1.6 N or 0.83%. The modal hammer standard deviations are also improved with a value of approximately 3 N.

In order to compute the model's energy dissipation, a displacement ring-down is needed from the experiment. By first integrating the measured velocity signal with respect to time using a trapezoidal numerical integration, one can approximate the measured displacement signal. Using the same data processing technique as discussed above, the modal displacement ring-down was also obtained and averaged. The displacement ring-down is used to compare the dissipation model (Eq. 6) to the measured experimental data (Eq. 16).

OPTIMIZING MODEL PARAMETERS

The damping parameters $\{F_S, K_T, K_\infty, \chi, \beta, C\}$ of the modal model, seen in Fig. 1, were fit to experimental data using several different optimization routines. The objective function is posed as:

$$\text{Min } f = f_D + f_K \tag{19}$$

where

$$f_D = \left(\frac{D_{Experiment} - D_{Model}}{\max\left(D_{Experiment} - D_{Model}\right)} \right)^2 \quad (20)$$

and

$$f_K = \left(\frac{K_{Experiment} - K_{Model}}{\max\left(K_{Experiment} - K_{Model}\right)} \right)^2 \quad (21)$$

Note that the dissipation and stiffness objective functions, f_D and f_K respectively, are weighted so that their values are on the order of 1.

The nonlinear objective function, Eq. 19, can be optimized using either local or global optimization. Both techniques were explored by the authors in this work; however, when multiple local minima exist, local optimization algorithms tended to be highly dependent on the starting guess. Therefore, a global optimization algorithm (the DIRECT algorithm developed by Jones et al. [17]) was used to provide a more robust approach to optimizing the parameters. In addition, local optimization routines were used in MATLAB (fminsearch, fmincon, lsqnonlin [18]) to fine tune the solution and ensure convergence. Even with the global optimization algorithm, it was important to have a reasonable starting guess. For this work, starting guesses for the $\{F_S, K_T, K_\infty, \chi, \beta\}$ parameters were found using the graphical approach described in [6].

The graphical approach that was used to deduce the starting values will be summarized briefly, assuming the experimental energy dissipated per cycle, D_{Exp}, and stiffness, K_{Exp}, have been obtained from a set of measurements using the approach described in [16]. The energy dissipation per cycle and stiffness can be plotted versus the modal force which, with mass normalized mode shapes, is equal to the modal acceleration $\ddot{q}$. The χ parameter is found by fitting a line to the data for the log of energy dissipation versus log of the modal force at low force levels. Then the χ parameter for each mode r is given by:

$$\chi_r = \text{Slope}_r - 3 \quad (22)$$

In order to deduce the modal Iwan stiffness, K_T, the natural frequencies of each mode are plotted versus modal joint force. A softening of the system, characterized by a drop in frequency, illustrates the amount of modal stiffness associated with all the relevant joints of the system. The equation for modal joint stiffness for each mode becomes

$$K_{T,r} = K_{0,r} - K_{\infty,r} = \omega_{0,r}^2 - \omega_{\infty,r}^2 \quad (23)$$

where ω_0 is the natural frequency corresponding to the case when all the joints in the structure exhibit no slipping, and ω_∞ is the natural frequency when all of the joints are slipping. However, macro-slip was not clearly observed at the force levels tested so ω_∞ values were assumed to be slightly lower than the lowest measured omega value.

The modal joint slip force, F_S, can be estimated from the modal force level at which the stiffness or frequency begins to drop. To find the last parameter, β, all of the previous parameters found are needed along with the y-intercept, A, of the line that was fit in order to find the χ parameter. Then, the following equation was formed from [2] that can be used to solve for β_r numerically.

$$F_{S,r} = \left[\frac{4\left(\chi_r + 1\right) K_{T,r}^{\chi_r+2} \left(\beta_r + \frac{\chi_r + 1}{\chi_r + 2} \right)^{\chi_r+1}}{A_r K_{\infty,r}^{(3+\chi_r)} \left(2+\chi_r\right)\left(3+\chi_r\right)\left(1+\beta_r\right)^{\chi_r+2}} \right]^{\frac{1}{\chi_r+1}} \quad (24)$$

Finally, a reasonable starting guess for the modal viscous damping parameter, C, can be obtained from the modal damping ratios presented in Table 3 with $C = 2m\zeta\omega_0$.

RESULTS

The measurements from the beam were band-pass filtered and averaged as described previously to isolate the first bending mode of the beam, with the bolts tightened to 3.39 N-m. The optimization procedure was then used to find the modal parameters that best fit the data both with and without the additional viscous damping term. The model without the viscous damper relies entirely on the Iwan joint to dissipate energy. The parameters of the optimized models are shown in Table 5.

Table 5: Optimized parameters of the first bending mode of vibration at a bolt torque of 3.39 N-m, for the modal models with and without the viscous damper.

Parameter	Iwan Model	Iwan & Viscous Damper Model
F_S	6.23	2.33
K_T	$2.61 \cdot 10^5$	$1.37 \cdot 10^5$
K_∞	$3.19 \cdot 10^5$	$4.41 \cdot 10^5$
χ	-0.272	-0.178
β	0.836	0.0316
C	N/A	3.96

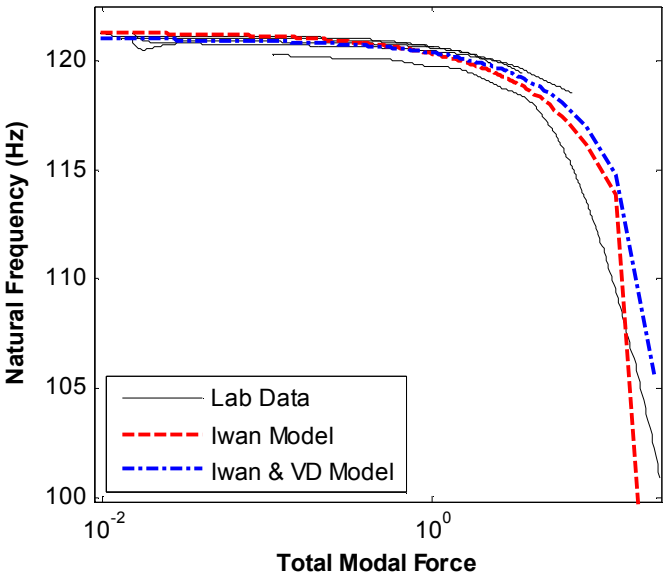

Fig. 4 Frequency comparison of two optimized modal models to experimental data.

Fig. 4 shows the natural frequency of the modal Iwan model versus the total modal force for the two modal models, reconstructed using Eq. (7). The measurements show that the natural frequency of this mode changes approximately 20 Hz over the range of forces that were applied. Both models seem to be capable of capturing the change in natural frequency over this range. Unfortunately, the natural frequency is not observed to level off at ω_∞ so it appears that the system never completely reaches macro slip .

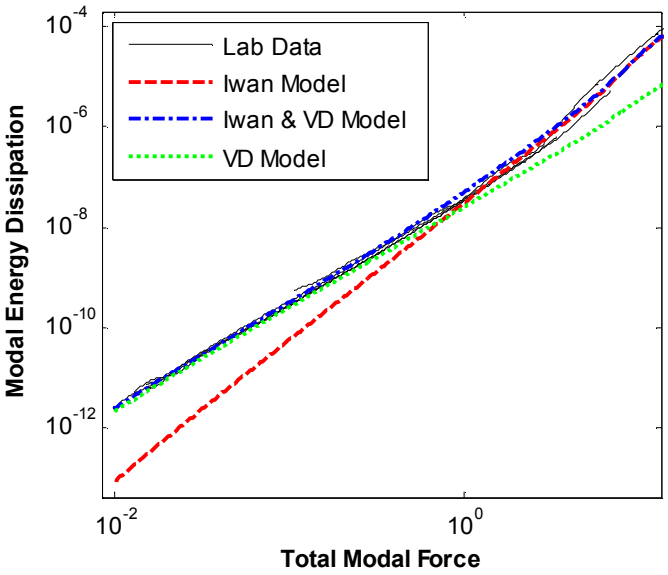

Fig. 5 Energy dissipation comparison of two optimized modal models to experimental data over a range of forces.

Fig. 5 shows the modal energy dissipation versus total modal force for the two modal models and the experimental data at five different excitation levels. The Iwan model without a viscous damper in parallel fails to fit the measurements at low amplitude, while the model with only a viscous damper does not capture the increase in damping at high forces. (Because of the logarithmic scale, the difference at high force levels may appear to be small yet the linear model is significantly in error at high force levels.) In contrast, the modal Iwan model with a viscous damper in parallel provides an excellent approximation to the measured energy dissipation. It should also be noted that the disagreement seen when the Iwan model was used alone does not appear to be due to the choice of parameters. Considerable effort was spent to optimize that model's parameters to better match the measurements, yet the fit could not be improved without decreasing the agreement of the natural frequency versus force plot in Fig. 4. This difficulty disappeared when a viscous damper was added to the model.

The differences between these models is more easily visualized by comparing the slope of the energy dissipation versus force curve. As mentioned previously, a single Iwan joint exhibits a slope of $3+\chi$ on a log dissipation versus log force plot. Fig. 6 compares the slope of the two optimized modal models with the experimentally measured slope. A fifth order polynomial was fit to the to the laboratory data in order to compute its slope. Also, it should be noted that the the Iwan models with and without the viscous damper are optimized to this polynomial fitted line. Without an additional viscous damper, the modal Iwan model has a much larger slope than the laboratory data at low force levels. On the other hand, when a viscous damper is added in parallel with the Iwan joint, the slope follows the laboratory data more closely over the entire range of force levels.

Note that the optimized models have identified a value for the slip force, F_S, that is in the range of the measured forces. Thus, at the highest measured force levels macro-slip has been initiated in both models. Unfortunately, the exciter that was used was not capable of even higher forces so macro-slip could not be fully characterized.

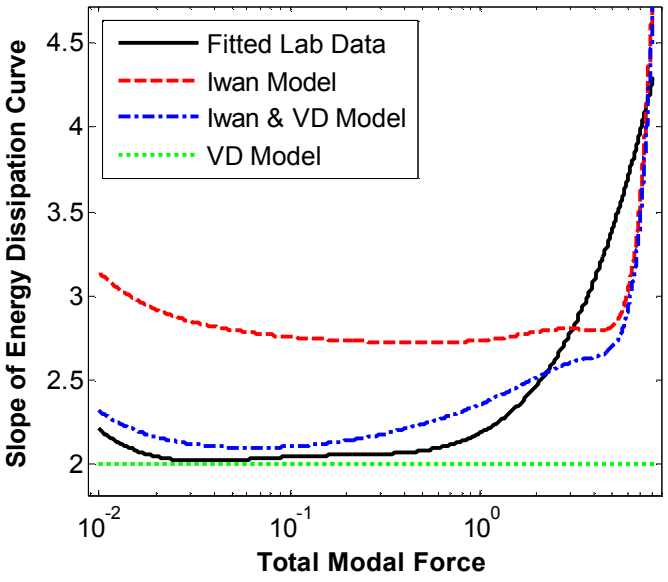

Fig. 6 Slope of energy dissipation versus modal force for modal Iwan models and a polynomial fit to the experimental measurements.

This same procedure was repeated for the first three elastic modes at three different bolt torques and the identified modal Iwan parameters are shown in Table 6. In general, the slip force parameter, F_S, tends to increases when the bolts are tightened for all modes considered. As the bolts are tightened, the preload in the bolts increases so larger forces are required to initiate macro-slip. As the bolts are tightened, one would expect that the K_∞ parameter for each mode would stay relatively constant while the joint stiffness, K_T, would increase. However, the optimized stiffness parameters, K_T and K_∞, seem not to follow much of a trend for this system. This probably indicates that the measured data is not adequate to reliably estimate K_∞, as might be expected since the excitation force was not sufficient to bring the system well into macro slip. The joint parameter, χ, can be observed to decrease as the bolt torques or stiffness of the system increased. Thus, the energy dissipation resembles a linear system at high bolt torques. Finally, the viscous damping parameter, C, seems to remain in a similar range for each mode considered. The equivalent low-amplitude damping ratio was computed for each case and these are also shown and they seem to be plausible lower bounds for the damping that noted in Table 3.

Table 6: Optimized parameters for a modal Iwan model with a viscous damper. First three elastic modes each at varying bolt torques.

Bolt Torque N-m (in-lbf)	**1.13 (10)**	**3.39 (30)**	**5.65 (50)**
1st Elastic Mode			
F_S	2.17	2.33	2.49
K_T	$1.03\cdot10^5$	$1.37\cdot10^5$	$1.01\cdot10^5$
K_∞	$5.16\cdot10^5$	$4.41\cdot10^5$	$4.79\cdot10^5$
χ	-0.115	-0.178	-0.437
β	$4.34\cdot10^{-4}$	0.0316	0.214
C	1.71	3.96	1.84
f_0 (Hz)	125.2	121.0	121.2
ζ (%)	0.083	0.199	0.092
2nd Elastic Mode			
F_S	0.739	1.07	1.18
K_T	$1.71\cdot10^5$	$1.63\cdot10^5$	$2.41\cdot10^5$
K_∞	$1.79\cdot10^6$	$1.66\cdot10^6$	$1.58\cdot10^6$
χ	-0.171	-0.428	-0.938
β	0.698	2.90	7.75
C	6.31	1.06	7.06
f_0 (Hz)	222.9	214.9	214.8
ζ (%)	0.172	0.030	0.200
3rd Elastic Mode			
F_S	0.966	1.39	1.02
K_T	$3.15\cdot10^5$	$2.86\cdot10^5$	$1.31\cdot10^5$
K_∞	$8.28\cdot10^6$	$8.58\cdot10^6$	$9.05\cdot10^6$
χ	-0.0550	-0.150	-0.286
β	0.471	0.164	0.00305
C	4.14	7.26	5.65
f_0 (Hz)	466.6	473.9	482.2
ζ (%)	0.054	0.093	0.071

CONCLUSION

In this work, a viscous damper was added in parallel with a modal Iwan model and a procedure was discussed to identify parameters for the model from laboratory data. The 4-parameter Iwan model was found to fit the measurements very well for the first three bending modes, suggesting that modal coupling was weak and that a modal Iwan model may be an effective way of accounting for the nonlinear damping associated with the mechanical joints of the system. The measurements also showed that it was important to also have a viscous damper in parallel with the Iwan element in order to account for the linear damping associated with the material and the boundary conditions. This modal Iwan approach is very appealing since it allows one to treat a structure as a set of uncoupled linear modes with slightly nonlinear characteristics in the micro-slip regime. There are only a few parameters to identify and the parameters χ, β, C and K_T are all fairly clearly represented in the modal response. On the other hand, in this study F_S and K_∞ were somewhat difficult to estimate since we were not able to apply large enough input forces to drive the system well into the macro-slip regime.

Work is under way to explore whether systems such as these system can be well modeled as having uncoupled modes of vibration as was done here. To date, the results suggest that this approach can be very successful until the structure reaches macro-slip and sometimes at surprisingly high force levels [6].

ACKNOWLEDGMENTS

The experimental work for this paper was conducted at Sandia National Laboratories. Sandia National Laboratories is a

multi-program laboratory managed and operated by Sandia Corporation, a wholly owned subsidiary of Lockheed Martin Corporation, for the U.S. Department of Energy's National Nuclear Security Administration under contract DE-AC04-94AL85000. The authors would especially like to thank Jill Blecke, Hartono Sumali, Randall Mayes, Brandon Zwink and Patrick Hunter for the help that they provided with the laboratory setup and testing.

REFERENCES

[1] D. J. Segalman, "An Initial Overview of Iwan Modelling for Mechanical Joints," Sandia National Laboritories, Albuquerque, New Mexico SAND2001-0811, 2001.

[2] D. J. Segalman, "A Four-Parameter Iwan Model for Lap-Type Joints," *Journal of Applied Mechanics,* vol. 72, pp. 752-760, September 2005.

[3] M. S. Allen and R. L. Mayes, "Estimating the degree of nonlinearity in transient responses with zeroed early-time fast Fourier transforms," *Mechanical Systems and Signal Processing,* vol. 24, pp. 2049-2064, 2010.

[4] D. J. Segalman and W. Holzmann, "Nonlinear Response of a Lap-Type Joint using a Whole-Interface Model," presented at the 23rd International Modal Analysis Conference (IMAC-XXIII), Orlando, Florida, 2005.

[5] D. J. Segalman, "A Modal Approach to Modeling Spatially Distributed Vibration Energy Dissipation," Sandia National Laboratories, Albuquerque, New Mexico and Livermore, California SAND2010-4763, 2010.

[6] B. J. Deaner, M. S. Allen, M. J. Starr, and D. J. Segalman, "Investigation of Modal Iwan Models for Structures with Bolted Joints," presented at the International Modal Analysis Conference XXXI, Garden Grove, California USA, 2013.

[7] Q. Zhang, Allemang, R. J. , Brown, D. L., "Modal Filter: Concept and Application," presented at the 8th International Modal Analysis Conference (IMAC VIII), Kissimmee, Flordia, 1990.

[8] S. D. Stearns, *Digital Signal Processing with Examples in Matlab*. New York: CRC Press, 2003.

[9] M. Feldman, "NON-LINEAR SYSTEM VIBRATION ANALYSIS USING HILBERT TRANSFORM - I. FREE VIBRATION ANALYSIS METHOD 'FREEVIB'," *Mechanical Systems and Signal Processing,* vol. 8, pp. 119-127, 1993.

[10] H. Sumali and R. A. Kellogg, "Calculating Damping from Ring-Down Using Hilbert Transform and Curve Fitting," presented at the 4th International Operational Modal Analysis Conference (IOMAC), Istanbul, Turkey, 2011.

[11] "Torque-Tension Tightening for Inch Series Fastners," in *Surface Vehicle Information Report*, ed: Society of Automotive Engineers (SAE) J1707-1999.

[12] T. G. Carne, D. T. Griffith, and M. E. Casias, "Support Conditions for Experimental Modal Analysis," *Sound and Vibration,* vol. 41, pp. 10-16, 2007.

[13] H. Sumali, "An experiment setup for studying the effect of bolt torque on damping," presented at the 4th International Conference on Experimental Vibration Analysis for Civil Engineering Structures (EVACES), Varenna, Italy, 2011.

[14] M. S. Allen and J. H. Ginsberg, "A Global, Single-Input-Multi-Output (SIMO) Implementation of The Algorithm of Mode Isolation and Applications to Analytical and Experimental Data," *Mechanical Systems and Signal Processing,* vol. 20, pp. 1090-1111, 2006.

[15] M. S. Allen and J. H. Ginsberg, "Global, hybrid, MIMO implementation of the algorithm of mode isolation," in *23rd International Modal Analysis Conference (IMAC XXIII)*, 2005.

[16] M. W. Sracic, M. S. Allen, and H. Sumali, "Identifying the modal properties of nonlinear structures using measured free response time histories from a scanning laser Doppler vibrometer," presented at the International Modal Analysis Conference XXX, Jacksonville, Florida USA, 2012.

[17] D. R. Jones, Perttunen, C. D., Stuckman, B. E., "Lipschitzian Optimization Without the Lipschitz Constant," *Journal of Optimization Theory and Application,* vol. 79, pp. 157-181, 1993.

[18] "Optimization Toolbox For Use with MATLAB," ed. Natick, MA: The MathWorks, Inc., 2003.

